

Very Large Interstellar Grains as Evidenced by the Mid-Infrared Extinction¹

Shu Wang^{1,2}, Aigen Li², and B.W. Jiang¹

ABSTRACT

The sizes of interstellar grains are widely distributed, ranging from a few angstroms to a few micrometers. The ultraviolet (UV) and optical extinction constrains the dust in the size range of a couple hundredth micrometers to several submicrometers. The near and mid infrared (IR) emission constrains the nanometer-sized grains and angstrom-sized very large molecules. However, the quantity and size distribution of micrometer-sized grains remain unknown as they are gray in the UV/optical extinction and they are too cold and emit too little in the IR to be detected by *IRAS*, *Spitzer*, or *Herschel*. In this work, we employ the $\sim 3\text{--}8\ \mu\text{m}$ mid-IR extinction which is flat in both diffuse and dense regions to constrain the quantity, size, and composition of the μm -sized grain component. We find that, together with nano- and submicron-sized silicate and graphite (as well as PAHs), μm -sized graphite grains with $\text{C}/\text{H} \approx 137$ ppm and a mean size of $\sim 1.2\ \mu\text{m}$ closely fit the observed interstellar extinction of the Galactic diffuse interstellar medium from the far-UV to the mid-IR as well as the near-IR to millimeter thermal emission obtained by *COBE/DIRBE*, *COBE/FIRAS*, and *Planck* up to $\lambda \lesssim 1000\ \mu\text{m}$. The μm -sized graphite component accounts for $\sim 14.6\%$ of the total dust mass and $\sim 2.5\%$ of the total IR emission.

Subject headings: dust, extinction — infrared: ISM — ISM: abundances

¹Department of Astronomy, Beijing Normal University, Beijing 100875, China; shuwang@mail.bnu.edu.cn, bjiang@bnu.edu.cn

²Department of Physics and Astronomy, University of Missouri, Columbia, MO 65211, USA; wan-shu@missouri.edu, lia@missouri.edu

¹Dedicated to the late Professor J. Mayo Greenberg (1922.1.14–2001.11.29) of Leiden University who first suggested the possible existence of very large grains in the interstellar space.

1. Introduction

The absorption and scattering — their combination is called “extinction” — of starlight are caused by interstellar grains of all sizes. But grains of sizes comparable to the wavelength (λ) of starlight absorb and scatter photons most effectively (i.e., $2\pi a/\lambda \sim 1$, where a is the spherical radius of the grain; see Li 2009). Because of this, interstellar grains have long been known to be “submicron-sized”, with a canonical size of $\sim 0.1 \mu\text{m}$ (i.e., $a \sim \lambda_V/2\pi \sim 0.1 \mu\text{m}$ for the visual band $\lambda_V = 5500 \text{ \AA}$) since their first detection via extinction and reddening in the visible (Trumpler 1930). However, it is now well recognized that they actually span a range of sizes from subnanometers (i.e., angstroms) and nanometers to submicrometers and micrometers.

The sub- μm -sized grain population is well constrained by the wavelength-dependent extinction from the near infrared (IR) at $\lambda < 3 \mu\text{m}$ to the far ultraviolet (UV) at $\lambda > 0.1 \mu\text{m}$. This population, ranging from a couple hundredth micrometers to several submicrometers, is often referred to as “sub- μm -sized” grains or “classical” grains.

The angstrom- and nano-sized grain population cannot be constrained even by the far-UV extinction. These grains (of sizes from $a < 50 \text{ \AA}$ down to a few angstroms) are often referred to as “very large molecules”, “very small grains” (VSG), “ultrasmall grains”, or “nanoparticles”. They are in the Rayleigh regime (i.e., $2\pi a/\lambda \ll 1$) in the far-UV. On a per unit volume (V) basis, their extinction cross section $C_{\text{ext}}(a, \lambda)$ of spherical radii a at wavelength λ is independent of grain size, i.e., $C_{\text{ext}}(a, \lambda)/V = C_{\text{ext}}(\lambda)/V$. The extinction resulting from these grains is not sensitive to the size distribution dn/da but their total volume:

$$\begin{aligned} A_\lambda/N_{\text{H}} &= 1.086 \int da \frac{1}{n_{\text{H}}} \frac{dn}{da} C_{\text{ext}}(a, \lambda) \\ &= 1.086 \frac{C_{\text{ext}}(\lambda)}{V} \int da \frac{1}{n_{\text{H}}} \frac{dn}{da} \frac{4\pi}{3} a^3 \\ &= 1.086 \frac{C_{\text{ext}}(\lambda)}{V} \left(\frac{V_{\text{VSG}}}{\text{H}} \right), \end{aligned} \quad (1)$$

where n_{H} (N_{H}) is the hydrogen volume (column) density, and V_{VSG}/H is the total volume per H nuclei of these grains. Eq.1 demonstrates that the observed far-UV extinction is not able to constrain the size distribution of this grain population. On the other hand, with a heat content smaller or comparable to the stellar photons that heat them, these grains are stochastically heated by single photons and do not attain an equilibrium temperature (Draine & Li 2001). Upon absorption of an energetic photon of energy $h\nu$, a ultrasmall grain will be heated to a maximum temperature T_p determined by its specific heat $C(T)$ and $h\nu$: $\int_0^{T_p} C(T) dT = h\nu$, and then rapidly radiates away most of the absorbed energy at

temperature T_p . Therefore, its IR emission contains crucial information about its size since $C(T) \propto a^3$ (see Li 2004). Indeed, as demonstrated by Li & Draine (2001; LD01) and Draine & Li (2007; DL07), the size distribution of the ultrasmall grain population is determined by the near- and mid-IR emission features at 3.3, 6.2, 7.7, 8.6 and 11.3 μm ascribed to polycyclic aromatic hydrocarbon (PAH), as well as the near- and mid-IR broadband photometry of *IRAS* and *COBE/DIRBE*, particularly those at $\lambda < 25 \mu\text{m}$.

In the UV/optical, micrometer-sized grains or “very large grains” (VLG) are in the geometrical-optics regime (i.e., $2\pi a/\lambda \gg 1$) and their extinction is essentially wavelength-independent or “gray” (Li 2009). Therefore, the UV/optical extinction is not able to constrain their quantity or size distribution. There are several lines of direct evidence for the presence of very large grains in the interstellar medium (ISM). Micrometer-sized interstellar SiC, graphite, Al_2O_3 , and Si_3N_4 grains have been found in primitive meteorites. They were identified as presolar grains of stellar origin based on their isotope anomalies (Clayton & Nittler 2004). Furthermore, the dust detectors aboard the *Ulysses* and *Galileo* spacecrafts have detected large interstellar grains with radii up to $\sim 2.0 \mu\text{m}$ flowing through the heliosphere from the local interstellar cloud (Grün et al. 1994, Krüger et al. 2007). Moreover, even *larger* interstellar grains (of radii $\sim 20 \mu\text{m}$) were detected as radar meteors entering the Earth’s atmosphere on solar-hyperbolic trajectories (Taylor et al. 1996, Baggaley 2000). More recently, Westphal et al. (2014) reported the detection of seven grains possibly of interstellar origin returned by the *Stardust* spacecraft (also see Sterken et al. 2015). These grains are mostly composed of Mg-rich silicates and three of them have radii $\gtrsim 1 \mu\text{m}$.

In addition, Witt et al. (2001) pointed out that the presence of very large grains in the ISM could be inferred from X-ray halos since the X-ray scattering efficiency varies approximately as a^4 while the differential cross section varies as a^6 . They examined the X-ray halo around Nova Cygni 1992 and found that, in order to explain the observed profile and intensity, the grain size distribution needs to extend to and possibly beyond $\sim 2 \mu\text{m}$. Furthermore, surprisingly high-albedo scattering at near-IR wavelengths has been reported for several dense regions (Witt et al. 1994, Block et al. 1994, Lehtinen & Mattila 1996), suggesting the possible presence of a population of grains at least $\sim 0.5 \mu\text{m}$ in radii. Moreover, based on the unaccounted for O/H abundance (Jenkins 2009, Whittet 2010), Jenkins (2009), Poteet et al. (2015), and Wang, Li & Jiang (2015) argued that the missing reservoir of O could reside on μm -sized H_2O grains. It is worth noting that four decades ago Greenberg (1974) had already pointed out that there could exist very large grains comprised of O, C, and N in the interstellar space. Socrates & Draine (2009) suggested that “pebble”-sized grains of $a \sim 1 \text{mm}$ may be detected through optical scattered light halos. Finally, we note that μm -sized grains were detected in dense cloud cores through the scattering of the interstellar radiation at the *Spitzer/IRAC* 3.6 and 4.5 μm bands (i.e., “coreshine”; Pagani et al.

2010, Steinacker et al. 2014).²

In this work, we aim at constraining the quantity and size distribution of the μm -sized dust population. This is achieved by fitting the observed mid-IR extinction at $\sim 3\text{--}8\ \mu\text{m}$ (§2) in terms of the silicate-graphite-PAH model together with an extra population of μm -sized grains (§3). We present the results in §4 and discuss their astrophysical implications in §5. Our principal conclusions are summarized in §6.

2. Mid-IR Extinction

The UV/optical interstellar extinction can be characterized by a single parameter R_V (Cardelli et al. 1989, CCM).³ The UV/optical extinction can be closely fitted in terms of the classical silicate-graphite model (Mathis et al. 1977, Draine & Lee 1984 [DL84]). In the IR at $1\ \mu\text{m} < \lambda < 7\ \mu\text{m}$, this model predicts a power-law extinction curve of $A_\lambda \propto \lambda^{-1.75}$ (Draine 1989). As elaborated in Wang, Li & Jiang (2014), this is too steep to be consistent with the subsequent observations made by the *Infrared Space Observatory* (ISO) and the *Spitzer Space Telescope*. Numerous observations suggest that the mid-IR extinction at $3\ \mu\text{m} < \lambda < 8\ \mu\text{m}$ is flat or “gray” for both diffuse and dense environments (see Figure 1), including the Galactic center (Lutz 1999, Nishiyama et al. 2009), the Galactic plane (Indebetouw et al. 2005, Jiang et al. 2006, Gao et al. 2009), the Coalsack nebula (Wang et al. 2013), and nearby star-forming regions (Flaherty et al. 2007). All these observations appear to suggest an “universally” flat mid-IR extinction law, with little dependence on environments.

3. Dust Model

We aim at reproducing the observed extinction from the UV/optical to the near- and mid-IR. We assume a mixture of amorphous silicate dust and carbonaceous dust, taking the size distribution functional form of Weingartner & Draine (2001; WD01). We assume that the latter extends from grains with graphitic properties at radii $a \gtrsim 50\ \text{\AA}$, down to grains with PAH-like properties at very small sizes (LD01). The WD01 model employs two log-normal

²The presence of this type of grains in dense environments is typically interpreted as due to grain growth which also occurs in proto-planetary disks (e.g., see Bouwman et al. 2001, Kessler-Silacci et al. 2006, Ricci et al. 2010). In contrast, those μm -sized grains discussed in this work are for the diffuse ISM as well, not confined to dense clouds.

³ $R_V \equiv A_V / (A_B - A_V)$ is the total-to-selective extinction ratio, where A_B is the blue band extinction at $\lambda_B = 4400\ \text{\AA}$. For the Galactic average, $R_V \approx 3.1$.

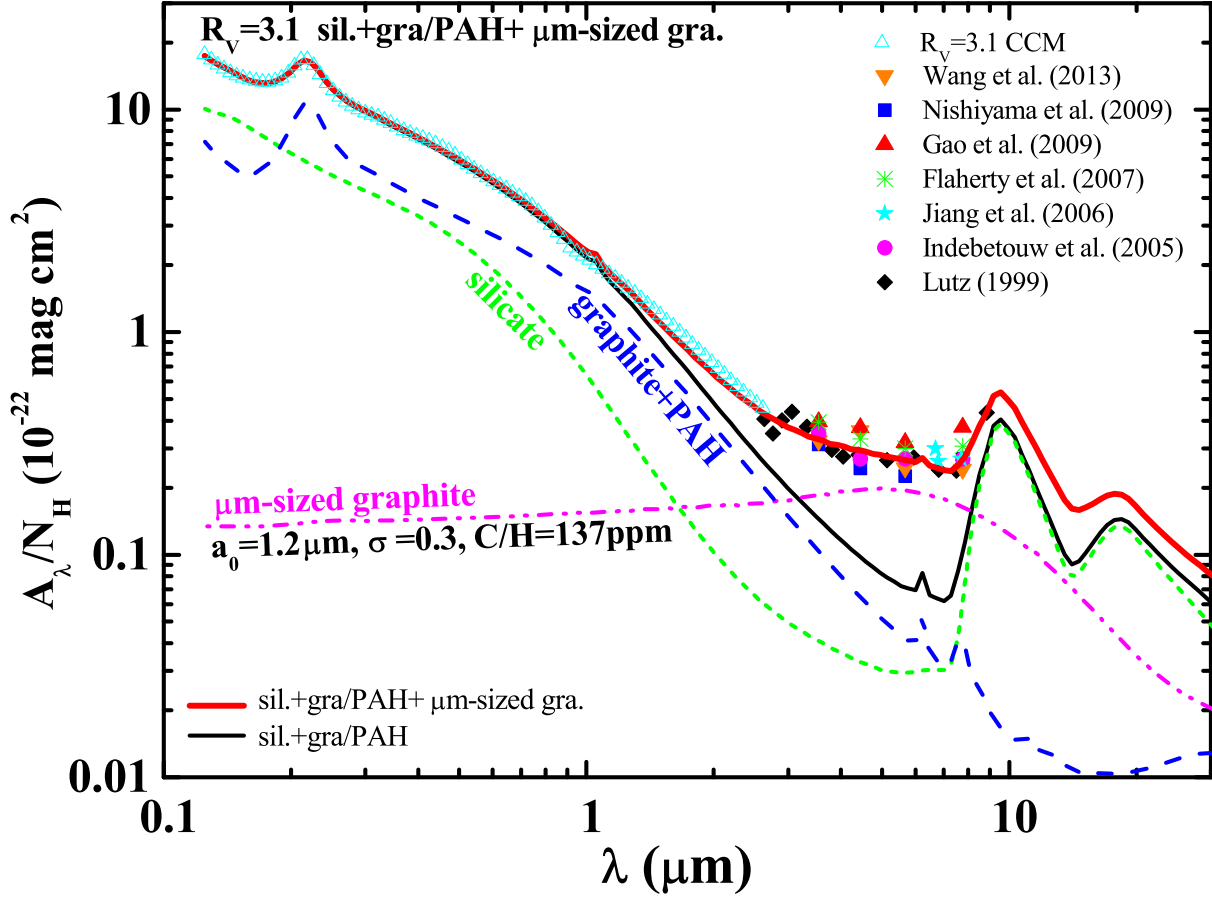


Fig. 1.— Fitting the $R_V = 3.1$ extinction curve from the UV/optical to the near- and mid-IR with (1) amorphous silicate (green short-dashed line), (2) graphite and PAHs (blue dashed line), and (3) μ m-sized graphite (magenta dash-dot-dotted line) with a log-normal size distribution characterized by $a_0 \approx 1.2 \mu\text{m}$, $\sigma \approx 0.3$, and $b_{\text{VLG}} \approx 137 \text{ ppm}$ (see eq. 2). The thick red solid line plots the model-fit which is the sum of silicate, graphite/PAHs, and μ m-sized graphite. The black solid line plots the sum of silicate and graphite/PAHs. The symbols plot the observed extinction: cyan open triangles plot the $R_V = 3.1$ UV/optical/near-IR extinction, while other symbols plot the mid-IR extinction (see text).

size distributions for two populations of PAHs which respectively peak at $a_{0,1}$, $a_{0,2}$ and have a width of σ_1 , σ_2 , consuming a C abundance of $b_{C,1}$, $b_{C,2}$ (per H nuclei). Following DL07, we adopt $a_{0,1} = 3.5 \text{ \AA}$, $\sigma_1 = 0.40$, $b_{C,1} = 45 \text{ ppm}$, $a_{0,2} = 20 \text{ \AA}$, $\sigma_2 = 0.55$, and $b_{C,2} = 15 \text{ ppm}$. These parameters were constrained by the observed near- and mid-IR emission. To account for the mid-IR extinction, we invoke an extra population of very large grains for which we

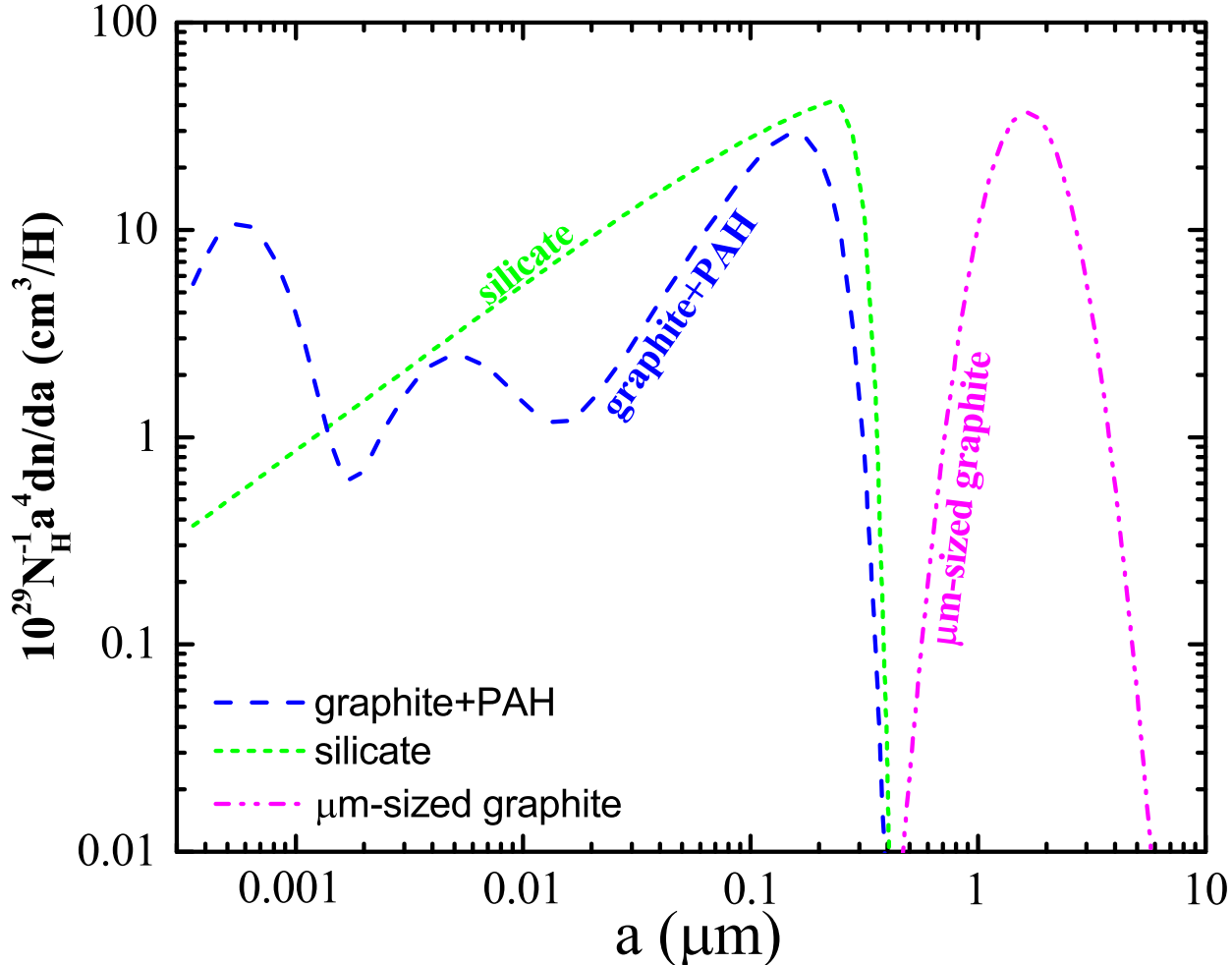


Fig. 2.— Grain size distributions for (1) silicate (green short-dashed line), (2) graphite and PAHs (blue dashed line), and (3) μm -sized “very large” graphite (magenta dash-dot-dotted line).

also adopt a log-normal size distribution of peak size a_0 and width σ :

$$\frac{1}{n_{\text{H}}} \frac{dn}{da} = \frac{3}{(2\pi)^{3/2}} \times \frac{\exp(-4.5\sigma^2)}{\rho a_0^3 \sigma} \times \frac{b_{\text{VLG}} \mu m_{\text{H}}}{2} \times \frac{1}{a} \exp \left\{ -\frac{1}{2} \left[\frac{\ln(a/a_0)}{\sigma} \right]^2 \right\}, \quad (2)$$

where m_{H} is the atomic H mass, ρ and μ are respectively the mass density and the molecular weight of the dust species ($\rho \approx 3.5 \text{ g cm}^{-3}$ and $\mu \approx 172$ for silicate, $\rho \approx 2.24 \text{ g cm}^{-3}$ and $\mu \approx 12$ for graphite), and b_{VLG} is the abundance per H nuclei locked up in μm -sized grains.

We consider 120 wavelengths, equally spaced in $\ln \lambda$, to model the extinction between $0.125 \mu\text{m}$ and $8 \mu\text{m}$. For the “observed” extinction in the wavelength range of $0.125 \mu\text{m} < \lambda < 3 \mu\text{m}$, we take the Galactic average of $R_V = 3.1$ as parameterized by CCM. For the $\sim 3\text{--}8 \mu\text{m}$ mid-IR extinction, we first obtain a weighted “average” from the observed extinction shown in Figure 1, with twice as much weight given to the diffuse sightlines toward the Galactic center. We then interpolate the “average” mid-IR extinction into 25 logarithmically equally-spaced wavelengths.

We take the optical constants of astronomical silicate and graphite of DL84. The PAH absorption cross sections are taken from DL07. Following WD01, we use the Levenberg-Marquardt method to minimize $\chi^2 = \chi_1^2 + \chi_V^2$, where χ_1^2 gives the error in the extinction fit:

$$\chi_1^2 = \sum_i \frac{[\ln A_{\text{obs}}(\lambda_i) - \ln A_{\text{mod}}(\lambda_i)]^2}{\sigma_i^2} \quad , \quad (3)$$

where $A_{\text{obs}}(\lambda_i)$ and $A_{\text{mod}}(\lambda_i)$ are respectively the observed and model-computed extinction at wavelength λ_i . Following WD01, we take the weights $\sigma_i^{-1} = 1$ for $0.125 \mu\text{m} < \lambda < 0.9 \mu\text{m}$ and $\sigma_i^{-1} = 1/3$ for $0.9 \mu\text{m} < \lambda < 8 \mu\text{m}$. The “penalty” term χ_V^2 prevents the model-consumed C and Si abundances ($[\text{C}/\text{H}]_{\text{dust}}$, $[\text{Si}/\text{H}]_{\text{dust}}$) from grossly exceeding their interstellar abundances:

$$\chi_V^2 = 0.4[\max(\tilde{\text{C}}, 1) - 1]^{1.5} + 0.4[\max(\tilde{\text{Si}}, 1) - 1]^{1.5} \quad , \quad (4)$$

where $\tilde{\text{C}} = [\text{C}/\text{H}]_{\text{dust}}/233 \text{ ppm}$ and $\tilde{\text{Si}} = [\text{Si}/\text{H}]_{\text{dust}}/36.3 \text{ ppm}$ (ppm is an abbreviation of parts per million).

4. Results

In fitting the far-UV to mid-IR extinction represented by 120 “data points” (see §3), we have ten parameters from the WD01 size distribution function (C_g , $a_{t,g}$, $a_{c,g}$, α_g , β_g for graphite, C_s , $a_{t,s}$, $a_{c,s}$, α_s , β_s for silicate) and three parameters from the μm -sized grain component. Following WD01, we fix $a_{c,s} = 0.1 \mu\text{m}$.⁴ We consider a graphite composition for the μm -sized grain component.⁵ As shown in Figure 1, with $a_0 \approx 1.2 \mu\text{m}$, $\sigma \approx 0.3$, and $b_{\text{VLG}} \approx 137 \text{ ppm}$, the observed extinction from the far-UV to the mid-IR is closely reproduced

⁴WD01 found that the fitting error only mildly varies with $a_{c,s}$ provided $a_{c,s} \lesssim 0.1 \mu\text{m}$ while it abruptly increases with $a_{c,s}$ when $a_{c,s} > 0.1 \mu\text{m}$.

⁵In the following, unless otherwise stated, we refer “graphite/PAHs” to nano- and sub- μm -sized graphitic grains (including PAHs).

(with $\chi^2 \approx 0.23$). The corresponding parameters for the WD01 size distribution function are: $C_g \approx 5.75 \times 10^{-12}$, $\alpha_g \approx -1.40$, $\beta_g \approx 0.0291$, $a_{t,g} \approx 0.00818 \mu\text{m}$, and $a_{c,g} \approx 0.173 \mu\text{m}$ for graphite, $C_s \approx 7.56 \times 10^{-14}$, $\alpha_s \approx -2.19$, $\beta_s \approx -0.586$, and $a_{t,s} \approx 0.204 \mu\text{m}$ for silicate. The derived size distributions are illustrated in Figure 2.

The model requires a total silicate mass (relative to H) of $M_{\text{sil}}/M_{\text{H}} \approx 6.95 \times 10^{-3}$, and a total carbonaceous dust mass (relative to H) of $M_{\text{carb}}/M_{\text{H}} \approx 4.34 \times 10^{-3}$, indicating a total gas-to-dust mass ratio of $M_{\text{gas}}/M_{\text{dust}} \approx 124$, where $M_{\text{gas}} \approx M_{\text{He}} + M_{\text{H}} \approx 1.4 M_{\text{H}}$ for $\text{He}/\text{H} \approx 0.1$. The required elemental depletions are $[\text{Si}/\text{H}]_{\text{dust}} \approx 40.4$ ppm and $[\text{C}/\text{H}]_{\text{dust}} \approx 362$ ppm. The latter includes $[\text{C}/\text{H}]_{\text{VLG}} \approx 137$ ppm in μm -sized graphite grains and $[\text{C}/\text{H}]_{\text{PAH}} = 60$ ppm in PAHs, which respectively account for $\sim 37.8\%$ and $\sim 16.6\%$ of the total mass of the carbonaceous dust component, and $\sim 14.6\%$ and $\sim 6.38\%$ of the total dust mass.

We have also tried μm -sized silicate grains. Compared with graphite, silicates are much more transparent at $\lambda < 8 \mu\text{m}$. To account for the observed mid-IR extinction, one requires $[\text{Si}/\text{H}]_{\text{VLG}} \approx 2.95 \times 10^4$ ppm to be locked up in μm -sized silicates, far exceeding the available amount of $[\text{Si}/\text{H}]_{\text{ISM}} \approx 32\text{--}41$ ppm in the ISM (see §5). Also, μm -sized silicate grains exhibit a Si–O resonance dip at $\sim 8 \mu\text{m}$ which is not seen in the observed extinction curve. We have also considered μm -sized iron grains. Unless they are extremely-elongated like needles (Dwek 2004), the mid-IR extinction requires a depletion of $[\text{Fe}/\text{H}]_{\text{VLG}} \approx 100$ ppm, far exceeding the available amount of $\text{Fe}/\text{H} \approx 28\text{--}35$ ppm in the ISM. More recently, Köhler et al. (2014) found that amorphous silicates with iron nanoparticles embedded could enhance the mid-IR extinction. Köhler et al. (2015) further found that dust aggregates could also cause increased mid-IR extinction. It would be interesting to see how their model extinction per H column compares with the observed extinction.

5. Discussion

5.1. IR Emission

As shown in Figure 1, μm -sized graphite grains are “gray” in the UV, optical, and near-IR. They do not absorb much in the UV/optical, and therefore by implication do not emit much radiation in the IR. We have calculated the temperature probability distribution functions of PAHs, small graphite and silicate grains of radii smaller than $\sim 250 \text{ \AA}$ which are heated by the Mathis, Mezger, & Panagia (1983, MMP83) interstellar radiation field (ISRF). We have also calculated the equilibrium temperatures of silicate and graphite grains of radii larger than $\sim 250 \text{ \AA}$ (see Figure 3). The resulting IR emission is shown in Figure 4

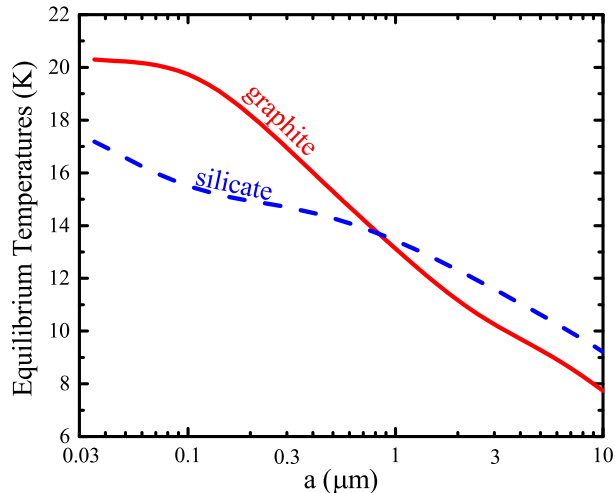


Fig. 3.— Equilibrium temperatures for silicate (dashed line) and graphite grains (solid line) heated by the MMP83 ISRF.

and compared with that of the diffuse ISM observed by *COBE*/DIRBE, *COBE*/FIRAS and *Planck*.⁶ Our model yields a total IR intensity of $\sim 4.55 \times 10^{-24} \text{ erg s}^{-1} \text{ H}^{-1}$. The fractional contributions of silicate, graphite/PAHs, and μm -sized graphite are approximately 27.5%, 70.0%, and 2.5%, respectively. The μm -sized graphite component is cold ($T \approx 13.1, 12.5, 11.2 \text{ K}$ for $a = 1, 1.2, 2 \mu\text{m}$ compared to $T \approx 20 \text{ K}$ for $a = 0.1 \mu\text{m}$, see Figure 3) and its contribution to the overall emission is only noticeable at $\lambda \gtrsim 550 \mu\text{m}$, becomes significant at $\lambda \gtrsim 1382 \mu\text{m}$, and dominates the emission at $\lambda \gtrsim 2098 \mu\text{m}$.

Figure 4 shows that our model fits the observed emission very well from the near-IR to submm: up to $\lambda \lesssim 850 \mu\text{m}$, it is in close agreement with the *COBE*/FIRAS spectrophotometry. At $\lambda > 850 \mu\text{m}$, the model emission slightly exceeds the *COBE*/FIRAS data. We note that the *Planck* photometric data at $\lambda \gtrsim 850 \mu\text{m}$ are also slightly higher than the *COBE*/FIRAS spectrophotometry. Our model is in excellent agreement with the *Planck* data up to $\lambda \gtrsim 1382 \mu\text{m}$, and does not overpredict until $\lambda \gtrsim 2098 \mu\text{m}$. At $\lambda = 3000 \mu\text{m}$, the model emission is stronger than the *COBE*/FIRAS photometry by a factor of ~ 1.5 and exceeds the *Planck* data by $\sim 72\%$. However, the far-IR dielectric functions of graphite and

⁶Many *Herschel* observations have been dedicated to the investigation of the dust properties in the ISM (e.g., see Abergel et al. 2010, Gordon et al. 2010, Molinari et al. 2010, Juvela et al. 2011, Juvela 2015). In this work, these *Herschel* data are not included since the *Herschel*/PACS bands are essentially covered by *COBE*/DIRBE, while the *Herschel*/SPIRE bands are essentially covered by *COBE*/FIRAS and *Planck* (see Table 4 of LD01 and Table 6 of DL07).

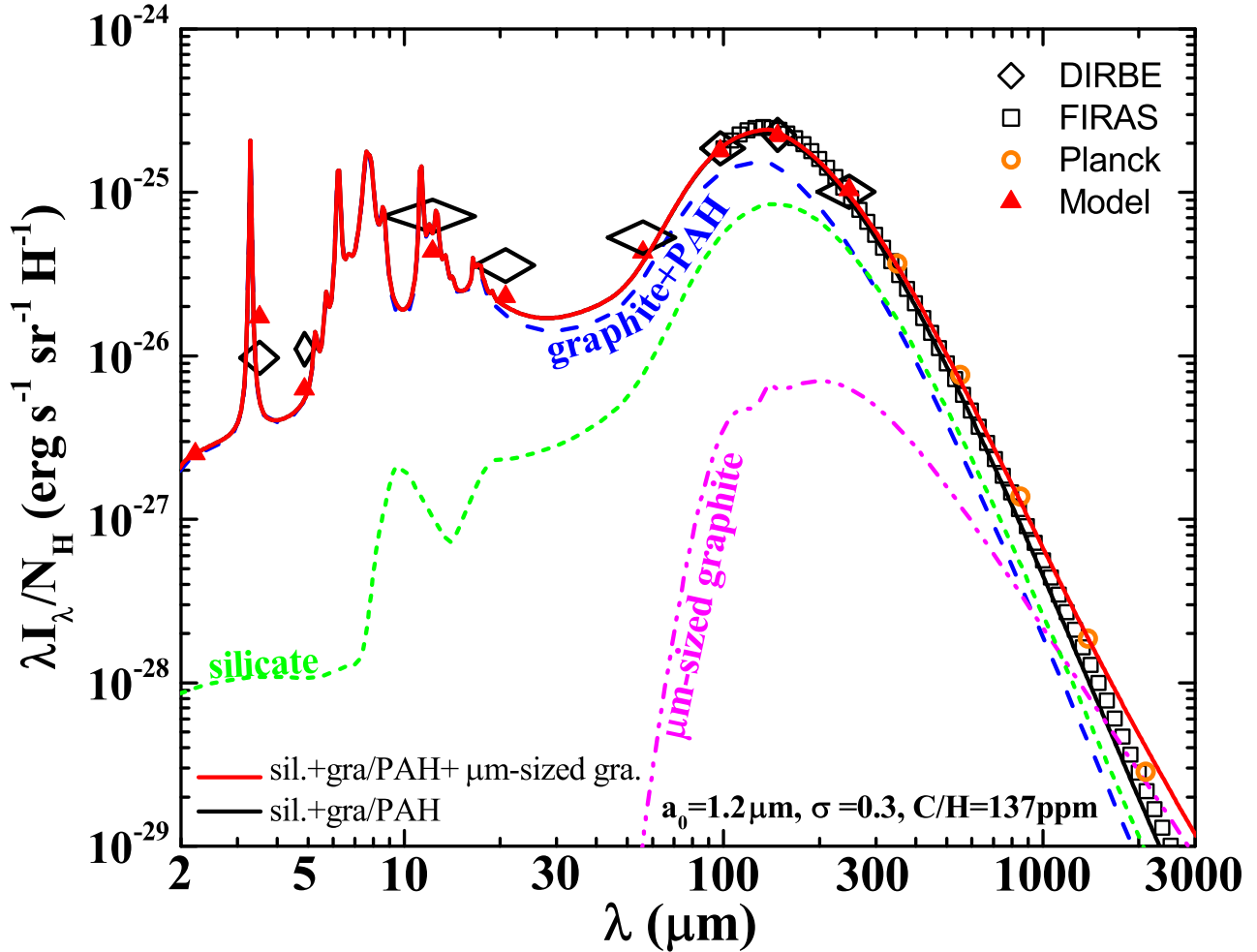


Fig. 4.— Comparison of the model to the observed emission from the diffuse ISM. Green short-dashed line shows emission from amorphous silicate; blue dashed line shows emission from graphite/PAHs; magenta dash-dot-dotted line shows emission from μm -sized graphite grains. Red triangles show the model spectrum (red solid line) convolved with the DIRBE filters. Observational data are from DIRBE (black diamonds; Arendt et al. 1998), FIRAS (black squares; Finkbeiner et al. 1999), and Planck (orange circles; Planck Collaboration XVII 2014).

silicate adopted here may not be known with a high precision (e.g., at $\lambda = 1000 \mu\text{m}$ the DL84 silicate has an opacity of $\kappa_{\text{abs}} \approx 0.33 \text{ cm}^2 \text{ g}^{-1}$, while the silicate material measured by Agladze et al. (1996) had $\kappa_{\text{abs}} \approx 1.25 \text{ cm}^2 \text{ g}^{-1}$). We also note that the *Planck* data at $\lambda = 3000 \mu\text{m}$ exceeds that of *COBE*/FIRAS by $\sim 45\%$.

Finkbeiner, Davis & Schlegel (1999; FDS) approximated the *COBE*/FIRAS data in terms of a two-component model consisting of a warm component of temperature $T_W \approx 16.2$ K and a cold component of temperature $T_C \approx 9.4$ K: $I_\lambda \sim \lambda^{-2.70} B_\lambda(T_W) + 0.47 \lambda^{-1.67} B_\lambda(T_C)$. They ascribed the warm component to carbonaceous grains and the cold component to amorphous silicates. We argue that while the FDS two-component model provides an excellent representation of the observed far-IR emission, their ascription may not be physical. As shown in Figure 3, to attain an equilibrium temperature of $T_C = 9.4$ K, silicate grains need to be very large, with radii $a \approx 8.9 \mu\text{m}$. Such very large silicate grains are gray in the UV/optical and contribute little to the UV/optical extinction. As a result, the observed UV/optical extinction would exclusively rely on carbonaceous dust. However, it is known that neither silicates nor carbonaceous dust *alone* can account for the observed UV/optical extinction (see Li 2005a). It is more natural to attribute the warm component to a combination of sub- μm -sized silicate and carbonaceous grains and the cold component either to a population of μm -sized grains or alternatively, according to the two-level-system (TLS) model, to the low energy transitions associated with the disordered internal structure of sub- μm -sized amorphous grains (Meny et al. 2007).

A cold emission component of $T \sim 4\text{--}7$ K was also noted in the *COBE*/FIRAS Galactic emission spectrum by Wright et al. (1991) and Reach et al. (1995). Rowan-Robinson (1992) explained the cold emission in terms of grains of $a = 30 \mu\text{m}$. But he did not specify the composition of this grain population. He simply assumed its absorption efficiency to be $Q_{\text{abs}}(a, \lambda) = 1$ for $\lambda < 4\pi a$ and $Q_{\text{abs}}(a, \lambda) = 4\pi a/\lambda$ for $\lambda \geq 4\pi a$.

As shown in Figure 4, our model SED flattens at $\lambda \gtrsim 1382 \mu\text{m}$. The overall dust opacity at $\lambda < 1382 \mu\text{m}$ has a power-index of $\beta_{\text{FIR}} \approx 1.89$. In contrast, the opacity at $\lambda > 1382 \mu\text{m}$ has a slightly smaller power-index of $\beta_{\text{mm}} \approx 1.67$. The *Planck* observations of the Galactic diffuse ISM detected the flattening of the SED at long wavelengths, with $\beta_{\text{FIR}} - \beta_{\text{mm}} \approx 0.15$ at $\lambda > 850 \mu\text{m}$ (see Planck Collaboration XVII 2014). These observations also provided evidence for the far-IR opacity variations in the diffuse ISM, attributable to large amorphous carbon grains or the TLS model of disordered charge distribution in amorphous grains.

5.2. The C/H Crisis

The interstellar abundances of Si/H and C/H are unknown. They are often assumed to be that of solar ($[\text{Si}/\text{H}]_\odot \approx 32.4 \pm 2.2$ ppm, $[\text{C}/\text{H}]_\odot \approx 269 \pm 31$ ppm, Asplund et al. 2009), proto-Sun ($[\text{Si}/\text{H}]_\odot \approx 40.7 \pm 1.9$ ppm, $[\text{C}/\text{H}]_\odot \approx 288 \pm 27$ ppm, Lodders 2003), early B stars ($[\text{Si}/\text{H}]_\star \approx 31.6 \pm 3.6$ ppm, $[\text{C}/\text{H}]_\star \approx 214 \pm 20$ ppm, Nieva & Przybilla 2012), or young F/G stars ($[\text{Si}/\text{H}]_\star \approx 39.9 \pm 13.1$ ppm, $[\text{C}/\text{H}]_\star \approx 358 \pm 82$ ppm, Sofia & Meyer

2001). Our model consumes $[\text{Si}/\text{H}]_{\text{dust}} \approx 40.4$ ppm which is consistent with the proto-Sun Si/H abundance. With the gas-phase abundance of $[\text{C}/\text{H}]_{\text{gas}} \approx 140$ ppm (Cardelli et al. 1996) or $[\text{C}/\text{H}]_{\text{gas}} \approx 100$ ppm (Sofia et al. 2011) subtracted, the proto-Sun reference standard leaves only ~ 148 ppm or ~ 188 ppm of C/H for the dust, respectively. With $[\text{C}/\text{H}]_{\text{dust}} \approx 362$ ppm, our model uses too much C compared to what would be available in the ISM. Even ignoring the μm -sized graphite component, the silicate-graphite-PAH model, with $[\text{C}/\text{H}]_{\text{dust}} \approx 252$ ppm (WD01), is already in “C crisis” (Snow & Witt 1995). With the inclusion of a population of μm -sized graphite grains, our model amplifies the so-called “C crisis”.

The “C crisis” holds for all dust models, including that of Zubko et al. (2004; ZDA) which requires $[\text{C}/\text{H}]_{\text{dust}} \approx 244$ ppm (and $[\text{Si}/\text{H}]_{\text{dust}} \approx 36$ ppm) and Jones et al. (2013; J13) which requires $[\text{C}/\text{H}]_{\text{dust}} \approx 233$ ppm (and $[\text{Si}/\text{H}]_{\text{dust}} \approx 50$ ppm). Note that the mid-IR extinction has not been accounted for by ZDA or J13. The ZDA model produces much less extinction at $\lambda > 1 \mu\text{m}$ than observed (see Figure 23.11 in Draine 2011). The J13 model fitted the IR extinction tabulated in Mathis (1990) which is much lower than the mid-IR extinction described here in §2. The total consumed C/H is expected to be similar to ours if the flat mid-IR extinction is to be accounted for by their models. This is indicated by the Kramers-Kronig relation of Purcell (1969) which relates the wavelength-integrated extinction to the dust quantity: $\int_0^\infty A_\lambda/N_{\text{H}} d\lambda = 1.086 \times 3\pi^2 F (V_{\text{dust}}/\text{H})$ where V_{dust}/H is the total dust volume per H nucleon, and F is a dimensionless factor which depends only upon the grain shape and the static dielectric constant of the grain material. Spherical silicates ($F \approx 0.64$) with the proto-Sun abundance contribute $\approx 6.53 \times 10^{-26} \text{ mag cm}^3 \text{ H}^{-1}$ to the extinction integration. With $\int_{912\text{\AA}}^{1000\mu\text{m}} A_\lambda/N_{\text{H}} d\lambda \approx 1.70 \times 10^{-25} \text{ mag cm}^3 \text{ H}^{-1}$ (see Figure 1), one derives $[\text{C}/\text{H}]_{\text{dust}} \approx 365$ ppm for spherical graphite ($F \approx 1.0$). This is a lower limit since $\int_0^\infty A_\lambda/N_{\text{H}} d\lambda > \int_{912\text{\AA}}^{1000\mu\text{m}} A_\lambda/N_{\text{H}} d\lambda$. For moderately elongated grains, the C crisis still persists (e.g., with an elongation of ~ 2 – 3 , one requires $[\text{C}/\text{H}]_{\text{dust}} \approx 275$ ppm of graphite of $F \approx 1.25$).

A likely solution to the C crisis problem is that the stellar photospheric abundances of dust-forming elements may be considerably lower than that of the interstellar material from which young stars are formed. This could be caused by an incomplete incorporation of heavy elements in stars during the star formation process, and/or an underestimation of the degree of heavy-element settling in stellar atmospheres (see Li 2005b). Parvathi et al. (2012) derived the gas-phase C/H abundance of 16 Galactic interstellar sightlines. They found that $[\text{C}/\text{H}]_{\text{gas}}$ varies from one sightline to another, with $\sim 1/3$ of the sightlines having their gas-phase C/H abundance *alone* exceeding the proto-Sun C/H abundance (e.g., the sightline toward HD 206773 has a gas-phase C/H abundance of $\approx 464 \pm 57$ ppm [see Parvathi et al. 2012] which is comparable to the total C/H abundance of ~ 462 ppm required by our

model (i.e., $[C/H]_{\text{dust}} \approx 362$ ppm [see §4] plus $[C/H]_{\text{gas}} \approx 100$ ppm [see Sofia et al. 2011]).⁷

5.3. An Artificial Gap in the Grain Size Distribution?

The size distribution derived for the μm -sized dust component is not a continuous extension of the sub- μm -sized component but has a gap in between (see Figure 2). This seems inconsistent with the observed continuous size distribution of the interstellar grains entering the solar system (see Figure 2 of Frisch et al. 1999). However, the extinction resulting from such a continuous size distribution would be totally unlike what is actually observed (see Figures 3, 4 of Draine 2009).⁸ As a matter of fact, a close inspection of the *in situ* dust size distribution of Frisch et al. (1999) reveals that it already shows a flattening off at $a \gtrsim 0.5 \mu\text{m}$. Witt et al. (2001) also noted that the size distribution continuously extending to micrometers required to explain the X-ray halo around Nova Cygni 1992 would lead to an extinction curve with $R_V \approx 6.1$. It would be interesting to see if a size distribution with a gap in between the sub- μm -sized grains and the μm -sized grains like the one derived here could reproduce the observed X-ray halo and result in an extinction curve with $R_V \approx 3.1$.

5.4. The Origin of Very Large Grains

The origin of μm -sized interstellar grains is not known. Theoretical calculations show that carbon dust can grow to sizes as large as a few micrometers in the radioactive environment of supernova ejecta, even if O is more abundant than C (Clayton et al. 1999). These calculations are also applicable to the formation of μm -sized oxides within supernova gas having $C > O$. However, we do not know in the ISM how much dust originates from supernovae. If a substantial fraction of interstellar dust is from supernova condensates, then μm -sized grains may be prevalent in the ISM.

⁷If we attribute the flat $\sim 3\text{--}8 \mu\text{m}$ mid-IR extinction to μm -sized silicate or iron spheres, we would face a much more severe Si or Fe “crisis”: as discussed in §4, while the model consisting of μm -sized graphite grains requires $\sim 60\%$ more C/H than the proto-Sun C/H abundance, the model consisting of μm -sized silicate grains requires ~ 725 times more Si/H than the proto-Sun Si/H abundance, and the model consisting of μm -sized iron spheres requires ~ 3.0 times more Fe/H than the proto-Sun Fe/H abundance.

⁸Draine (2009) added a population of large grains to the WD01 size distribution so that the new one approximately reproduces that of the interstellar grains detected by *Ulysses* and *Galileo* at $m > 3 \times 10^{-13}$ g of Landgraf et al. (2000). With the inclusion of these large grains, Draine (2009) derived an extinction curve of $R_V \approx 5.8$.

We note that the size and quantity derived for the μm -sized graphite dust does not rely on the silicate-graphite-PAH model. The μm -sized component is inferred from the mid-IR extinction which is essentially independent of the observed properties (e.g., UV/optical/near-IR extinction, near-, mid-, and far-IR emission) previously used to constrain dust models. These models differ from each other in detailed composition and morphology (see Li 2004). But they all fit the UV/optical extinction and are deficient in comparison with the observed $\sim 3\text{--}8\ \mu\text{m}$ mid-IR extinction except the WD01 $R_V = 5.5$ model. To account for the observed mid-IR extinction, a population of μm -sized dust is required by all dust models. The size is inferred from a general consideration of light scattering theory. The quantity of this component can be inferred from the Kramers-Kronig relation of Purcell (1969).

Finally, we note that, while the μm -sized dust component derived here is carbonaceous in nature, the μm -sized interstellar grains detected by the *Stardust* spacecraft are remarkably devoid of carbon (Westphal et al. 2014). This is probably due to the shock destruction of carbonaceous grains in the local interstellar cloud, as revealed by the overabundant CII in the interstellar gas surrounding the heliosphere (see Slavin & Frisch 2008).

6. Summary

The $\sim 3\text{--}8\ \mu\text{m}$ mid-IR extinction is observed to be flat or gray in various interstellar environments, including low-density diffuse clouds, translucent clouds, and dense clouds. It provides a sensitive constraint on very large, μm -sized grains which are gray at optical wavelengths and whose existence can not be constrained by the far-UV to near-IR extinction. We model the flat $\sim 3\text{--}8\ \mu\text{m}$ mid-IR extinction with μm -sized grains together with a mixture of silicate and graphite grains of sizes ranging from a few angstroms to a few submicrometers. Our principal results are as follows:

1. The observed interstellar extinction is closely reproduced from the far-UV to the mid-IR with $[\text{Si}/\text{H}]_{\text{dust}} \approx 40.4\ \text{ppm}$ in silicate grains, $[\text{C}/\text{H}]_{\text{dust}} \approx 362\ \text{ppm}$ in carbonaceous grains which include PAHs ($[\text{C}/\text{H}]_{\text{PAH}} \approx 60\ \text{ppm}$), submicron-sized graphite ($\text{C}/\text{H} \approx 165\ \text{ppm}$), and μm -sized graphite ($[\text{C}/\text{H}]_{\text{VLG}} \approx 137\ \text{ppm}$). The sizes of the μm -sized graphite component are modeled as a log-normal distribution peaking at $a_0 \approx 1.2\ \mu\text{m}$ and having a width of $\sigma \approx 0.3$.
2. Our model closely reproduces the IR emission of the diffuse ISM observed by *COBE*/DIRBE, *COBE*/FIRAS, and *Planck* from the near-IR up to $\lambda \gtrsim 1382\ \mu\text{m}$. With equilibrium temperatures of $T \lesssim 13\ \text{K}$, μm -sized graphite grains dominate the emission at $\lambda \gtrsim 2098\ \mu\text{m}$ and account for $\sim 2.5\%$ of the total IR emission.

3. A carbon budget problem does arise with respect to our model when one compares the model-required C depletion of $[C/H]_{\text{dust}} \approx 362$ ppm with the solar and proto-Sun abundances of $[C/H]_{\odot} \approx 269, 288$ ppm.
4. Micrometer-sized silicate or iron grains, if present in the ISM, are unlikely responsible for the observed $\sim 3\text{--}8\ \mu\text{m}$ extinction as they would require too much Si/H and Fe/H, exceeding the proto-Sun Si/H and Fe/H abundances by a factor of ~ 725 and 3.0, respectively.

We thank A.C.A. Boogert, J. Gao, B.W. Holwerda, J.Y. Seok, V.J. Sterken, A.N. Witt, Y.X. Xie, and the anonymous referee for helpful comments/suggestions. This work is supported by NSFC 11173007, 11373015, 973 Program 2014CB845702, NSF AST-1109039, and NNX13AE63G. S.W. acknowledges support from the China Scholarship Council (No. 201406040138).

REFERENCES

- Abergel, A., Arab, H., Compiègne, M., et al. 2010, *A&A*, 518, L96
- Agladze, N. I., Sievers, A. J., Jones, S. A., et al. 1996, *ApJ*, 462, 1026
- Arendt, R. G., Odegard, N., Weiland, J. L., et al. 1998, *ApJ*, 508, 74
- Asplund, M., Grevesse, N., Sauval, A.J., & Scott, P. 2009, *ARA&A*, 47, 481
- Baggaley, W. J. 2000, *J. Geophys. Res.*, 105, 10353
- Block, D. L., Witt, A. N., Grosbol, P., et al. 1994, *A&A*, 288, 383
- Bouwman, J., Meeus, G., de Koter, A., et al. 2001, *A&A*, 375, 950
- Cardelli, J. A., Clayton, G. C., & Mathis, J. S. 1989, *ApJ*, 345, 245 (CCM)
- Cardelli, J. A., Meyer, D. M., Jura, M., & Savage, B. D. 1996, *ApJ*, 467, 334
- Clayton, D. D., Liu, W., & Dalgarno, A. 1999, *Science*, 283, 1290
- Clayton, D. D., & Nittler, L. R. 2004, *ARA&A*, 42, 39
- Draine, B. T. 1989, in *Infrared Spectroscopy in Astronomy*, ed. B. H. Kaldeich (Paris: ESA Publ. Division), 93

- Draine, B. T. 2009, *Space Sci. Rev.*, 143, 333
- Draine, B. T. 2011, *Physics of the Interstellar and Intergalactic Medium* (Princeton, NJ: Princeton Univ. Press)
- Draine, B. T., & Lee, H. M. 1984, *ApJ*, 285, 89 (DL84)
- Draine, B. T., & Li, A. 2001, *ApJ*, 551, 807
- Draine, B. T., & Li, A. 2007, *ApJ*, 657, 810 (DL07)
- Dwek, E. 2004, *ApJ*, 611, L109
- Flaherty, K. M., Pipher, J. L., Megeath, S. T., et al. 2007, *ApJ*, 663, 1069
- Finkbeiner, D. P., Davis, M., & Schlegel, D. J. 1999, *ApJ*, 524, 867 (FDS)
- Frisch, P. C., Dorschner, J. M., Geiss, J., et al. 1999, *ApJ*, 525, 492
- Gao, J., Jiang, B.W., & Li, A., 2009, *ApJ*, 707, 89
- Gordon, K. D., Galliano, F., Hony, S., et al. 2010, *A&A*, 518, L89
- Greenberg, J. M. 1974, *ApJ*, 189, L81
- Grün, E., Gustafson, B., Mann, I., et al. 1994, *A&A*, 286, 915
- Indebetouw, R., Mathis, J. S., Babler, B. L., et al. 2005, *ApJ*, 619, 931
- Jenkins, E. B. 2009, *ApJ*, 700, 1299
- Jiang, B.W., Gao, J., Omont, A., Schuller, F., & Simon, G. 2006, *A&A*, 446, 551
- Jones, A. P., Fanciullo, L., Köhler, M., et al. 2013, *A&A*, 558, A62 (J13)
- Juvela, M., Ristorcelli, I., Pelkonen, V.-M., et al. 2011, *A&A*, 527, A111
- Juvela, M. 2015, *Planet. Space Sci.*, in press
- Kessler-Silacci, J., Augereau, J.-C., Dullemond, C. P., et al. 2006, *ApJ*, 639, 275
- Köhler, M., Jones, A., & Ysard, N. 2014, *A&A*, 565, L9
- Köhler, M., Ysard, N., & Jones, A. P. 2015, *A&A*, 579, A15
- Krüger, H., Landgraf, M., Altobelli, N., et al. 2007, *Space Sci. Rev.*, 130, 401

- Landgraf, M., Baggaley, W. J., Grün, E., Krüger, H., & Linkert, G. 2000, *J. Geophys. Res.*, 105, 10343
- Lehtinen, K., & Mattila, K. 1996, *A&A*, 309, 570
- Li, A. 2004, in *ASP Conf. Ser. 309, Astrophysics of Dust*, ed. A. N. Witt, G. C. Clayton, & B. T. Draine (San Francisco, CA: ASP), 417
- Li, A. 2005a, *J. Phys.: Conf. Ser.*, 6, 229
- Li, A. 2005b, *ApJ*, 622, 965
- Li, A. 2009, in *Small Bodies in Planetary Sciences*, ed. I. Mann, A. Nakamura, & T. Mukai (Berlin: Springer), 167
- Li, A., & Draine, B. T. 2001, *ApJ*, 554, 778 (LD01)
- Lodders, K. 2003, *ApJ*, 591, 1220
- Lutz, D. 1999, in *The Universe as Seen by ISO*, ed. P. Cox & M. Kessler (ESA Special Publ., Vol. 427; Noordwijk: ESA), 623
- Mathis, J. S., Mezger, P. G., & Panagia, N. 1983, *A&A*, 128, 212 (MMP83)
- Mathis, J. S., Rumpl, W., & Nordsieck, K. H. 1977, *ApJ*, 217, 425
- Meny, C., Gromov, V., Boudet, N., et al. 2007, *A&A*, 468, 171
- Molinari, S., Swinyard, B., Bally, J., et al. 2010, *PASP*, 122, 314
- Nieva, M. F., & Przybilla, N., 2012, *A&A*, 539, 143
- Nishiyama, S., Tamura, M., Hatano, H., et al. 2009, *ApJ*, 696, 1407
- Pagani, L., Steinacker, J., Bacmann, A., et al. 2010, *Science*, 329, 1622
- Parvathi, V. S., Sofia, U. J., Murthy, J., & Babu, B. R. S. 2012, *ApJ*, 760, 36
- Planck Collaboration XVII 2014, *A&A*, 566, A55
- Poteet, C. A., Whittet, D. C. B., & Draine, B. T. 2015, *ApJ*, 801, 110
- Purcell, E. M. 1969, *ApJ*, 158, 433
- Reach, W. T., Dwek, E., Fixsen, D. J., et al. 1995, *ApJ*, 451, 188

- Ricci, L., Testi, L., Natta, A., & Brooks, K. J. 2010, *A&A*, 521, A66
- Rowan-Robinson, M. 1992, *MNRAS*, 258, 787
- Slavin, J. D., & Frisch, P. C. 2008, *A&A*, 491, 53
- Snow, T. P., & Witt, A. N. 1995, *Science*, 270, 1455
- Socrates, A., & Draine, B. T. 2009, *ApJ*, 702, L77
- Sofia, U. J., & Meyer, D.M., 2001, *ApJ*, 554, L221
- Sofia, U. J., Parvathi, V. S., Babu, B. R. S., & Murthy, J. 2011, *AJ*, 141, 22
- Steinacker, J., Ormel, C. W., Andersen, M., & Bacmann, A. 2014, *A&A*, 564, 96
- Sterken, V. J., Strub, P., Krüger, H., et al. 2015, *ApJ*, in press
- Taylor, A.D., Baggaley, W.J., & Steel, D.I., 1996, *Nature*, 380, 323
- Trumpler, R. J. 1930, *PASP*, 42, 214
- Wang, S., Gao, J., Jiang, B. W., Li, A., & Chen, Y. 2013, *ApJ*, 773, 30
- Wang, S., Li, A., & Jiang, B. W. 2014, *Planet. Space Sci.*, 100, 32
- Wang, S., Li, A., & Jiang, B. W. 2015, *MNRAS*, in press
- Weingartner, J. C., & Draine, B. T. 2001, *ApJ*, 548, 296 (WD01)
- Westphal, A. J., Stroud, R. M., Bechtel, H. A., et al. 2014, *Science*, 345, 786
- Whittet, D. C. B. 2010, *ApJ*, 710, 1009
- Witt, A. N., Lindell, R. S., Block, D. L., & Evans, Rh. 1994, *ApJ*, 427, 227
- Witt, A. N., Smith, R. K., & Dwek, E. 2001, *ApJ*, 510, L201
- Wright, E. L., Mather, J. C., Bennett, C. L., et al. 1991, *ApJ*, 381, 200
- Zubko, V., Dwek, E., & Arendt, R. G. 2004, *ApJS*, 152, 211 (ZDA)